Nat. Hazards Earth Syst. Sci., 14, 2079–2088, 2014
www.nat-hazards-earth-syst-sci.net/14/2079/2014/
doi:10.5194/nhess-14-2079-2014


Natural Hazards and Earth System Sciences
Open Access

# New improvement of the combined optical fiber transducer for landslide monitoring

**Z.-W. Zhu[1,2], Q.-Y. Yuan[3], D.-Y. Liu[1,2], B. Liu[4], J.-C. Liu[4], and H. Luo[1,2]**

[1]College of Civil Engineering of Chongqing University, Chongqing, 400045, China
[2]Key Laboratory of New Technology for Construction of Cities in Mountain Area, Chongqing University, Ministry of Education, Chongqing, 400045, China
[3]Department of Geriatrics, Southwest Hospital, the Third Military Medical University, Chongqing, 400038, China
[4]College of Electro-optic Engineering of Chongqing University, Chongqing, 400044, China

*Correspondence to:* Z.-W. Zhu (zqiao999@126.com)

Received: 10 May 2013 – Published in Nat. Hazards Earth Syst. Sci. Discuss.: 4 December 2013
Revised: 17 May 2014 – Accepted: 10 July 2014 – Published: 14 August 2014

**Abstract.** Landslide monitoring is important in predicting the behavior of landslides, thereby ensuring environmental, life, and property safety. On the basis of our previous studies, we conducted the double shear test by using a third-generation optical fiber transducer that uses expandable polystyrene (EPS) as base material. However, the third-generation transducer has poor performance when cohesive force is present between the grout and capillary stainless steel pipe of the transducer. Thus, the fourth-generation optical fiber transducer was invented. Similar to the third-generation transducer, the fourth-generation transducer also used EPS as its base material. Single shear test was conducted on the fourth-generation transducer after being grouted with cement mortar (1 : 1 mix ratio). The micro-bend loss mechanism of the optical fiber was considered, and the optical time domain reflectometry instrument was used. The fact that the loss sequence of optical fibers subjected to loading is different at various locations is found. The relationship of the loading-point displacement vs. optical fiber sliding distance and optical loss were measured. Results show that the maximum initial measurement precision of the newly proposed device is 1 mm, the corresponding sliding distance is 21 mm, and the dynamic range is 0–20 mm. The fourth-generation transducer can measure the movement direction of loadings, thus making this transducer applicable for landslide monitoring.

## 1 Introduction

There are many technologies to monitor landslides, such as global positioning system (GPS) (Jibson et al., 2000), remote sensing (RS) (Sun et al., 2003), digital close-range photogrammetry (Matori et al., 2012) for measuring ground surface displacement, and inclinometer (Sargand et al., 2004) and time domain reflectometry (TDR) (Dennis et al., 2006) for monitoring deep sliding surfaces. Methods that have employed optical fiber technologies such as optical time domain reflectometry (OTDR) (Higuchi et al., 2007; Tang et al., 2009), Brillouin optical time domain reflectometry (BOTDR) (Ding et al., 2005; Wang et al., 2009) and Brillouin optical time domain analysis (BOTDA) (Iten and Puzrin, 2009; Zeni, 2009) were also introduced into landslide monitoring area. However, all these present methods have advantages and disadvantages (Zhu et al., 2011).

In our previous studies, firstly, we reviewed the application of some electro-optic technologies (e.g., TDR, OTDR, BOTDR), in slope stability monitoring, and we point out that the electro-optic technologies are to become a new choice for slope stability monitoring (Zhu et al., 2009). Then, we designed a serial combined optical fiber transducer (COFT) to try to make this idea a reality. The first- and second-generation COFTs were made public in 2011 (Zhu et al., 2011). We employed the spatial construction principle of reinforced beams, the optical fiber micro-bending loss mechanism and OTDR technology. We used a base material, some capillary stainless steel pipes and optical fiber as the sensing

**Table 1.** Relevant parameters of EPS material.

| Parameter | Density ($kg\,m^{-3}$) | Initial elastic modulus (MPa) | Initial Poisson's ratio | Compressive strength (KPa) | Bending strength (KPa) | Tensile strength (KPa) |
|---|---|---|---|---|---|---|
| Value | 16 | 4.8 | 0.05 | 90 | 300 | 350 |

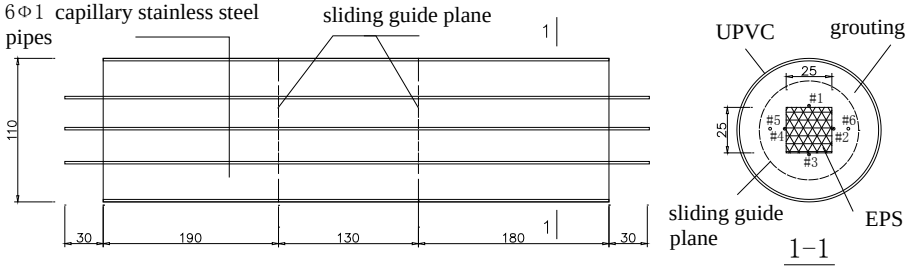


**Figure 1.** Double shearing test model (unit: mm).

element. Bending resistance tests were performed on the first- and second-generation transducers. Results showed that the performance of the first-generation COFT was poor. Its initial measurement precision and dynamic range were 5 mm and 0–7 mm, respectively. The performance of the second-generation COFT was better than that of the first-generation. Its initial measurement precision, sliding distance and dynamic range were 1.2, 21.8 and 0–20.6 mm, respectively. However, the second-generation COFT cannot measure the movement direction of loadings. So we designed the third-generation COFT. Bending resistance tests performed on the third-generation transducer grouted with concrete C40, and proved that such a sensor has higher initial measurement precision, larger sliding distance, and dynamic range.

Shearing force is the most common force exerted on the sliding plane during landslide. However, no evidence exists of whether transducers could achieve high initial measurement precision, large sliding distance and good dynamic range when these transducers are embedded in a grout and are subjected to shearing force. Considering this research limitation, we conducted double shearing tests by using the third-generation transducer grouted with cement. The third-generation transducer showed poor performance when cohesive force is present between the grout cement and the capillary stainless steel pipe, thereby compelling us to construct the fourth-generation transducer. To investigate the performance of this transducer under shearing force, shearing resistance tests were performed on two types of dimension of the fourth-generation transducer that was grouted with mortar. Laboratory results confirmed our previous assumptions and conclusions, such as higher initial measurement precision, the determination of the moving direction, etc.

## 2 Test on the third-generation transducer

### 2.1 Third-generation transducer

After several tests, expandable polystyrene (EPS) was selected as base material of the third-generation transducer. EPS was subsequently cut into rectangular parallelepipeds, and the cross sections of the parallelepipeds were shaped into squares. Φ1 capillary stainless steel pipes (#1, #2, #3, and #4) (Fig. 1) were arranged at the midpoint of each side. EPS is an ordinary commercial material in the market.

Table 1 shows the relevant parameters of the EPS (Wang and Wang, 2002). Capillary stainless steel pipes were purchased from Wenzhou BIZBAO Tube Manufacturer Co., Ltd. in Zhejiang Province, China. The pipes had 0.7 mm internal diameters, in which fiber optics penetrated through the pipes. The optical fiber used was a simple module (type G652B), which was purchased from Wuhan Yangtze Optical Fiber and Cable Co. Ltd, Wuhan, China. The diameter of the optical fiber was 245 µm.

### 2.2 Test model

We fabricated a cylinder test model by using an unplasticized polyvinyl chloride (UPVC) pipe as formwork. Table 2 shows the details of the cylinder test model.

Two 20 mm deep sliding guide planes, which were spaced 130 mm around the test piece, were created by using a cutting machine (Fig. 1). The distance of the two bearings of the test machine was set at 130 mm to guarantee the shearing movement of the test piece. To investigate the cohesive force between the mortar and the capillary stainless steel pipes, two Φ1 steel pipes (#5 and #6) that had no internal optical fibers were arranged beside the transducer.

**Table 2.** Parameters of test model.

| Test model | Dimension of the model (mm) | Cross section of the transducer (mm) | Grouting material | Curing time |
|---|---|---|---|---|
| 1 | $\Phi 110 \times 500$ | $25 \times 25$ | cement mortar 1 : 1 | 4 d |
| 2 | $\Phi 110 \times 500$ | $25 \times 25$ | cement mortar 1 : 2 | 14 d |
| 3 | $\Phi 110 \times 500$ | $25 \times 25$ | cement mortar 1 : 1 | 7 d |
| 4 | $\Phi 110 \times 500$ | $45 \times 45$ | cement mortar 1 : 1 | 21 d |

### 2.3 Other experimental materials and instruments

In this study, the experimental instruments we employed were the following: OTDR, type TFP2A, manufactured by Tektronix in the United States; optical fiber fusion splicer, type AV6491E, manufactured by the 41st Institute of China Electronics Technology Group Corporation, Hefei, China; fiber cleaver, type MAX CI-01, manufactured in South Korea; fiber optic stripper, type Clauss CFS-2, manufactured in the US; 0–50 submeters; and Vernier caliper. The 10 kN hydraulic universal testing machine was used as loading machine for the tests.

### 2.4 Experimental results

The results are shown in Figs. 2 and 3 and Tables 3 and 4.

Results show that test model integrity worsens as grouting strength decreases. The recovery amount of the reference steel pipe was larger than the sliding distance of fiber #3. However, the recovery amount of the reference steel pipe was smaller than that of the other fibers. The reference pipe of model 1 was broken. In this study, model 1 had the highest strength. Cohesive force was also shown to be positively correlated to the model strength, thereby indicating that cohesive force influences the movement of steel pipes. The influence of cohesive force on steel pipes should be reduced.

The two results have a certain initial measurement precision, sliding distance, and dynamic range, thus making this transducer capable of monitoring shear deformation.

The fitting curve of the sliding distance and the vertical displacement at the loading point is linear, whereas that of fiber optic loss is nonlinear.

Fiber optic loss occurred in the following order: fiber #1, #2, #4, and #3. This indicates this cylinder test model can determine the movement direction of the loading is from fiber #1–3, which is actually the same as the loading direction.

The maximum loss of the two models is less than 5 dB, which is lower than that of the second-generation transducer. Model 2 has a maximum sliding distance of less than 8.5 mm and has a dynamic range even less than 0–7 mm. These results indicate the poor performance of the third-generation transducer grouted with concrete when subjected to shear load.

## 3 Study on the fourth-generation transducer

### 3.1 Fourth-generation transducer

We designed a fourth-generation fiber transducer with bowknot (Fig. 4) and established a single shearing test model to overcome the drawbacks caused by the cohesive force that verified in the third-generation transducer double-shearing tests, to improve the performance of the transducer when subjected to shear load, and to verify its determination of the loading direction. The material and shape of the base material of the fourth-generation transducer was the same as that of the third-generation sensor.

However, additional fixed devices were set in the $\Phi 1$ steel pipe fixed range, and $\Phi 2$ capillary stainless steel pipes were capped on the $\Phi 1$ steel pipes. Pipes were produced by the company BIZBAO. The internal diameters of the $\Phi 1$ and $\Phi 2$ capillary stainless steel pipes were 0.7 and 1.7 mm, respectively.

### 3.2 Single shearing test model

Two models (model 3 and 4) were made with the same mix ratio of cement mortar by using base materials with different dimensions. Table 2 provides the model details. We fabricated a cylinder test model that has UPVC pipe as formwork to ensure that the model is compatible with the field test (Fig. 5).

Monitoring becomes inaccurate because the cohesive force of cement mortar on capillary stainless steel pipes hinders the free movement of steel pipes. Therefore, the model shown in Fig. 5 was designed to enable the $\Phi 1$ steel pipe house a 300 mm long $\Phi 2$ steel pipe that is treated with surface painting before placing into the test model. The $\Phi 2$ steel pipe will be pulled out once cement mortar pre-hardens to ensure that the $\Phi 1$ steel pipe can move freely in the mortar. To guarantee the anchorage quality of $\Phi 1$ steel pipes in fixed range, we provided two additional fixed devices with anchor bars on each steel pipe. A reference steel pipe #5 is placed

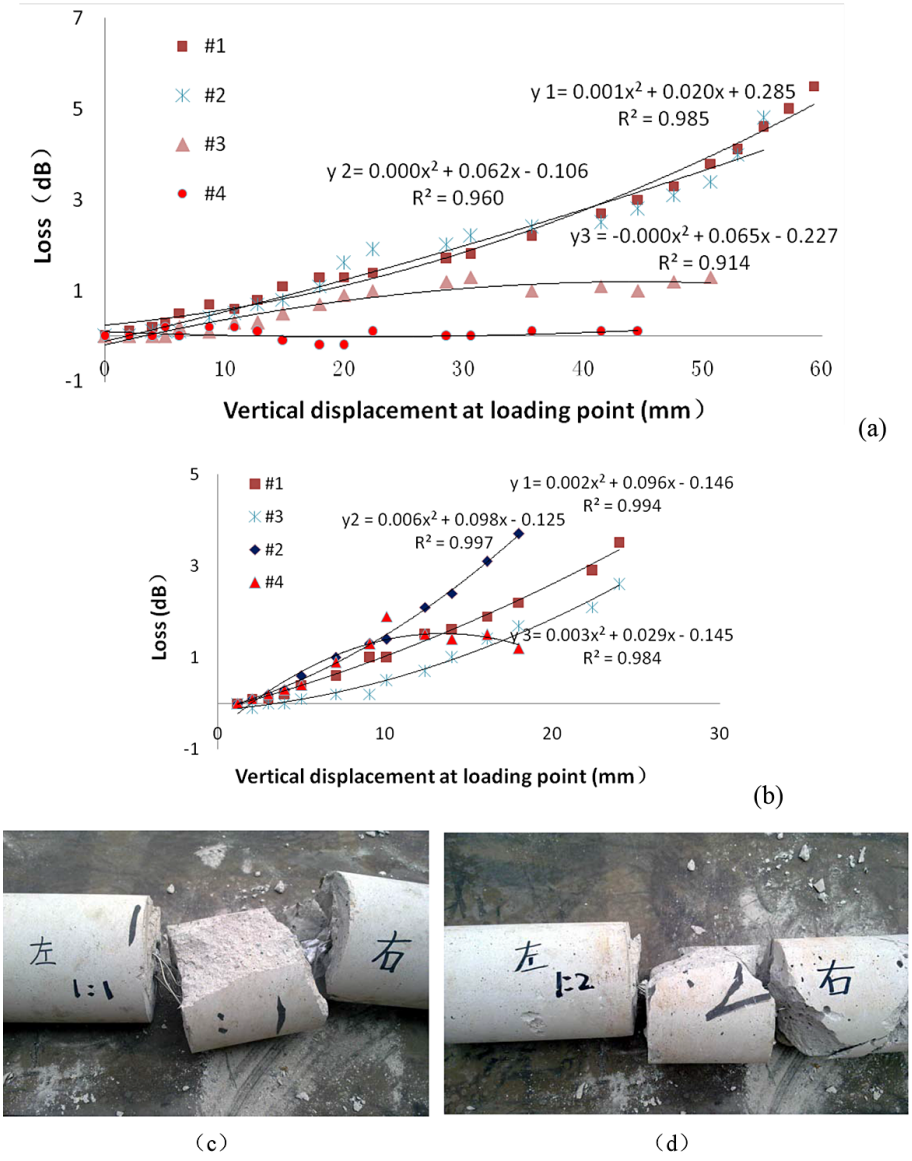


**Figure 2.** Results of double shearing tests. Relationship between fiber optical loss and vertical displacement at loading point. **(a)** Model 1, **(b)** model 2. Photos of model test completed. **(c)** Model 1, **(d)** model 2.

beside pipe #4 to verify the influence of cohesive force on the pipes.

### 3.3 Experiment

The simple shear model was adopted in the experiment. Once the test piece prehardens (after 3 days), a sliding guide plane that is 3 mm wide and 20 mm deep was cut perpendicularly in the axial direction by using a cutting machine (Fig. 5). The fixed end of the test piece was placed on the testing machine. The capillary stainless steel pipes were numbered in sequence (#1–4), each steel pipe was penetrated with optical fibers. A bowknot was formed at the free end of the test piece. The size of the bowknot was then adjusted, as shown in our previous studies (Zhu et al., 2011). Optical fibers were glued at the fixed end of the test piece by using 502-branded glue. A free optical fiber was set aside among each bowknot to ensure monitoring capabilities. The locations of the bowknot (left) and the Φ1 capillary stainless steel pipe (10 cm to the right) were marked to measure the distance traveled by the optical fibers. The universal tester was adjusted in the crown face of the test piece, and a dial indicator was installed to record the vertical displacement at the loading point. The optical fiber penetration test was performed prior to loading to guarantee optical fiber integrity and joint reliability. The length of the light waves in the experiment was 1310 nm.

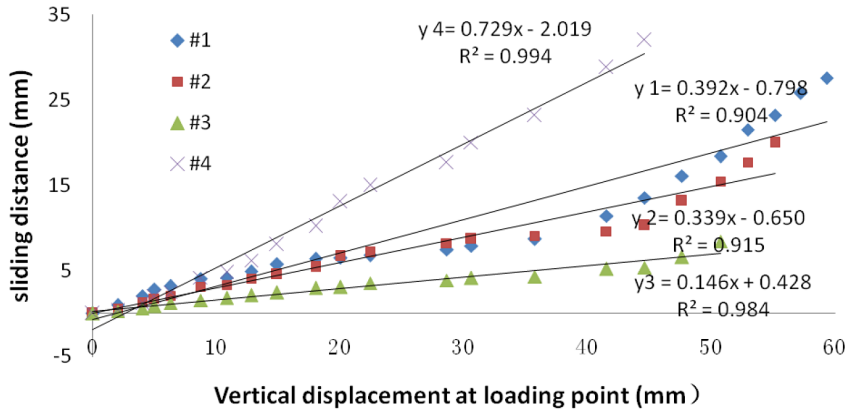


(a)

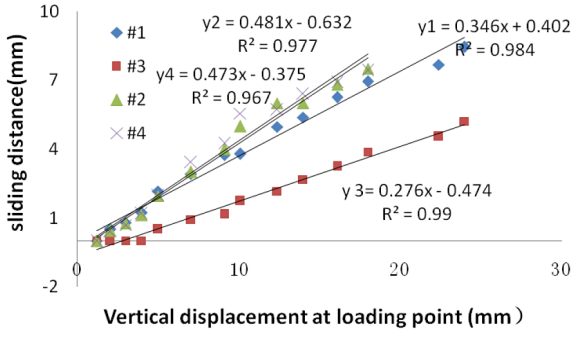


(b)

**Figure 3.** Relationship between fiber optical sliding distance and vertical displacement at loading point. **(a)** Model 1, **(b)** model 2.

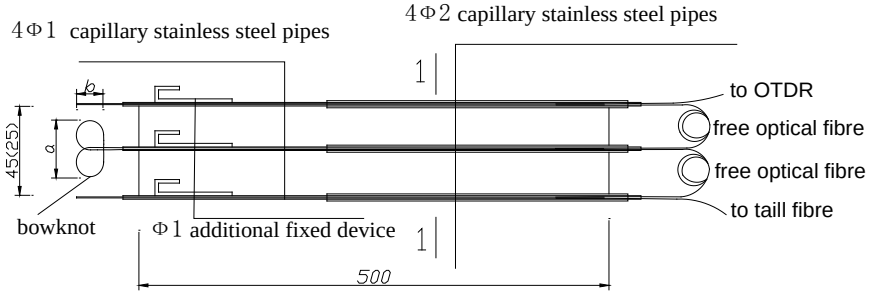


(a)

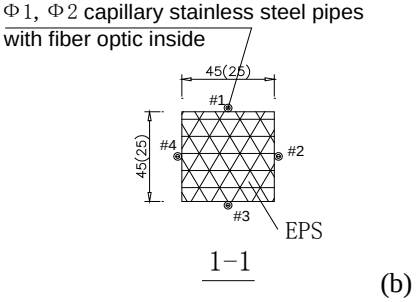


(b)

**Figure 4.** Draft of the fourth-generation transducer. **(a)** Elevation view of the Sensor. **(b)** Cross section of the sensor (unit: mm).

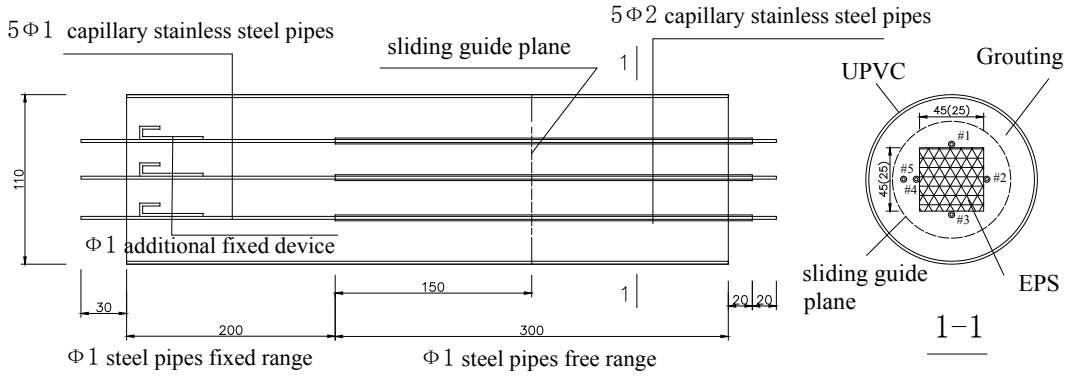


**Figure 5.** Single shearing test model (unit: mm).

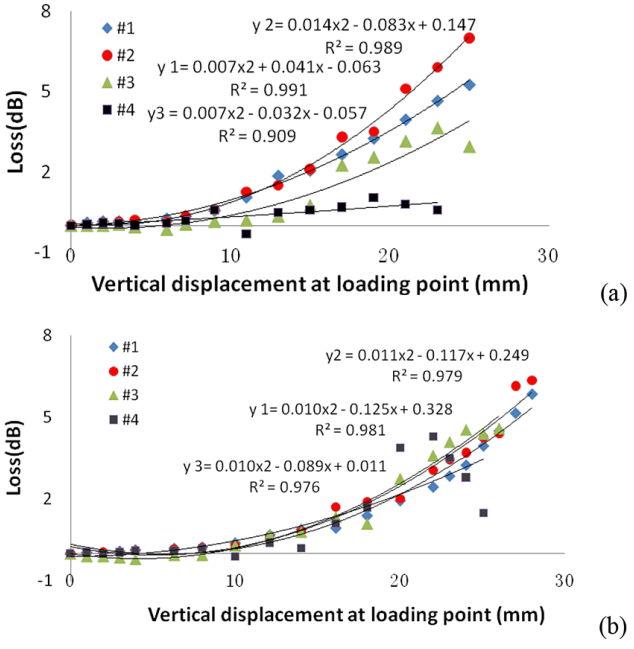


**Figure 6.** Relationship between fiber optical loss and vertical displacement at loading point. **(a)** Model 3, **(b)** model 4.

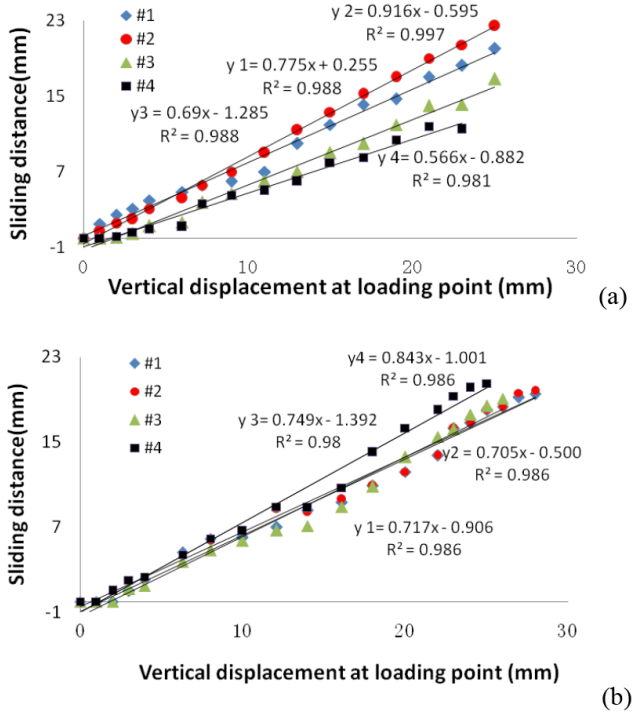


**Figure 7.** Relationship between fiber optical sliding distance and vertical displacement at loading point. **(a)** Model 3, **(b)** model 4.

### 3.4 Experimental results

Experimental results are shown in Figs. 6 and 7 and Tables 3 and 4.

At the end of the experiments, the test pieces were shown to be integral, and the reference pipes were not broken. The recovery amount of the reference steel pipe was close to the vertical displacement at loading point of both models. This result indicates that the influence of cohesive force between the steel pipes and mortar was reduced. The following indexes denote that the performance of the fourth-generation transducer with grouting is better than that of the third-generation transducer subjected to shearing force, thereby indicating the success of the design of the fourth-generation transducer.

Compared with model 4, model 3 had a higher initial measurement precision. When all the optical fibers of model 3 reached 0.1 dB, the corresponding relevant vertical displacements at the loading point were smaller than those of model 4. The highest initial measurement precision of model 3 reached 1 mm, which is smaller than that of the TDR technology (Dennis et al., 2006). The corresponding maximum sliding distance was 21 mm, which is higher than that of a single optical fiber (Tang et al., 2009). The fiber in the model was also not broken. The maximum sliding

**Table 3.** Catalogue of fiber optical maximum sliding distance and vertical displacement at loading point of each model.

| Test model | Fiber optical max. sliding distance (mm) | | | | Sliding value of reference pipe (mm) | Max. vertical displacement at loading point (mm) |
|---|---|---|---|---|---|---|
| | #1 | #2 | #3 | #4 | | |
| 1 | 27.56 | 19.98 | 8.46 | 31.98 | 16.56 | 59.3 |
| 2 | 8.44 | 7.5 | 5.22 | 7.42 | 6.16 | 24 |
| 3 | 21 | 23.6 | 16.8 | 11.5 | 25.08 | 26 |
| 4 | 20.9 | 22.76 | 19.1 | 20.5 | 28.32 | 29.1 |

distance of model 3 could be further increased. However, the test was interrupted because of the loss data in fibers #3 and #4, which were found to be saturated. The dynamic range of fibers #1 and #2 of model 3 reached 0–20 and 0–21.6 mm, respectively.

The sliding distances of the optical fiber around the transducer were smaller than the vertical displacement at the loading point. The differences of the sliding distances and the vertical displacement for fibers #1 and #3 were respectively greater than 20 and 30 % because of the influence of the soft base material.

The fiber optical losses for both models occurred in the following sequence: fiber #1, #2, #4, and #3. This result is similar to the results of the double shearing test. Thus, this model determined the loading direction is also from fiber #1–3.

The linear and nonlinear fitting curves of the fiber optical sliding distance and the loss and vertical displacements at loading point were similar to those of the double shearing test.

The performances of these two models were different. Therefore, model 3, which was grouted with a small-dimension transducer, was found to have good performance. Thus, model 3 is the better choice if the measurement range of the model is allowed.

## 4 Theoretical analysis of determination of loading direction

Assume that the loading direction is from pipe #1–3 and that the steel pipes of the fourth-generation transducer are arranged such that steel pipe #1 is at the near end adjacent to the detector, followed by #2 and #3 pipe, and finally #4 pipe. The shear failure mode of the beam should be used. Then shear stress, accompanied by tensile stress, will be produced first in steel pipe #1. Then pipes #2 and #4 will also be under shear stress. The EPS material is too soft, thus delaying pipe #3 in transferring a part of shear force. So, among the pipes, pipe #3 was under the least stress and was the last pipe to be subjected to stress.

When the loading direction of the subjected transducer is the same as that shown in Fig. 8, the force applied on the

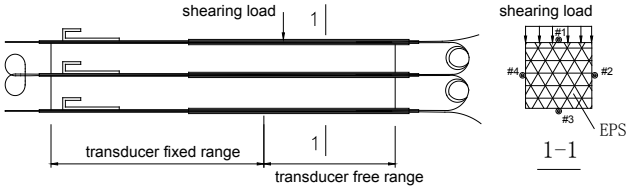


**Figure 8.** Diagram of the transducer subjected to shearing load.

transducer will cause sliding of steel pipes at the free end. As optical fibers are penetrated through the pipes, the stress on the pipes will be transferred to the optical fibers, and the pipe movement will lead to the sliding of optical fibers. The size of the bowknot at the free end of the optical fibers will decrease, and the optical fiber curvature will increase. These changes in the curvature will result in micro-bend loss, which will be captured by using the OTDR instrument. Therefore, the movement direction of loadings can be determined according to the sequence of occurrence of optical fiber loss. This result indicates that the movement direction starts from pipe #1 and ends at pipe #3, which is similar to the experimental results.

## 5 Discussion

The combined optical fiber transducer we invented is used for field monitoring of slope stability. The characteristic parameters (e.g., strength and friction angle) of the monitored slopes are different. For a given slope, in order to ensure successful monitoring, the transducer we invented must be suitable for those parameters. That is, the base material of the transducer, as well as its dimension, and grouting strength must be matched with the parameters of the given slope. Thus, these are discussed in the following subsections.

### 5.1 Influence of grouting strength

The experimental results showed that the integrity of model 1 is better than that of model 2 because the grout strength of model 1 is stronger than that of model 2. However, one

**Table 4.** Catalogue of initial measurement precision and dynamic range of each model.

| Test model | 1 | | | | 2 | | | | 3 | | | | 4 | | | |
|---|---|---|---|---|---|---|---|---|---|---|---|---|---|---|---|---|
| Number of optical fiber | #1 | #2 | #3 | #4 | #1 | #2 | #3 | #4 | #1 | #2 | #3 | #4 | #1 | #2 | #3 | #4 |
| Initial measurement precision value (mm) | 2 | 4 | 6.25 | 5 | 2.05 | 2.05 | 5 | 2.05 | 1 | 2.5 | 9 | 2.5 | 3 | 3.95 | 10 | 3.95 |
| Relevant loss (dB) | 0.2 | 0.1 | 0.2 | 0.2 | 0.1 | 0.1 | 0.1 | 0.1 | 0.1 | 0.12 | 0.35 | 0.11 | 0.1 | 0.1 | 0.3 | 0.1 |
| Dynamic range (mm) | 0–25.56 | 0–15.98 | 0–2.21 | 0–26.98 | 0–6.39 | 0–5.45 | 0–0.22 | 0–5.37 | 0–20 | 0–21.1 | 0–7.8 | 0–9 | 0–18.9 | 0–18.81 | 0–9.1 | 0–16.55 |

**Table 5.** Comparison of the present model with other monitoring models.

| Testing method | Precision of initial measurement | | Max. sliding distance | | Dynamic range (mm) | Determination of the loading direction | Unit price (USD $m^{-1}$) |
|---|---|---|---|---|---|---|---|
| | Value (mm) | Reflectometry coefficient/loss | Value (mm) | Reflectometry coefficient/loss | | | |
| TDR (Dennis et al., 2006) | 5 | 0.005 ($\rho$) | 25.4 | 0.123 ($\rho$) | 0–20.4 | Cannot | 13.5 |
| Single optical fiber (Tang et al., 2009) | 0.3 | 0.5 (dB) | 3.6 | 54 (dB) | 0–3.3 | Cannot | 0.03 |
| Method in our previous study (Zhu et al., 2011) | 2.3 | 0.11 (dB) | 26.5 | 9.1 (dB) | 0–23.2 | Cannot | 0.15 |
| The fourth-generation transducer | 1 | 0.1 (dB) | 21 | 5.95 (dB) | 0–20 | Can | 0.2 |

reference pipe of model 1 was broken. The positive correlation of cohesive force with grout strength leads to the reference pipe being broken.

Dennis et al. (2006) had carried out field monitoring on the slopes beside the Arkansas State Highway designated as Interstate 540 (I-540), which connects Fort Smith to Fayetteville, USA. Two field monitoring sites – mile marker 46 and mile marker 50 of I-540 – were set. Field monitoring results show that the weak grout at mile marker 50 did not cause TDR cable deformation. However, the grout was too strong to split the surrounding soil at mile marker 46. Therefore, the influence of grout strength should be fully considered.

### 5.2 Influence of base material

The transducer we invented did not confine the type and dimension of the base material of the transducer. We have studied the performance of the transducer that has EPS and polyvinyl chloride as base material, and various dimensions of the third-generation transducer were also employed. However, shearing tests were not conducted. Experimental results of this paper indicate that the performance of model 3 is better than that of model 4. The cement mortar ratio of the two models is the same. The sliding guide planes decrease much influence of curing time on mortar strength. The only difference found between the two models is their cross-section dimension of the two transducers. Thus, the performance of the transducer using various base materials and dimensions should be further studied.

### 5.3 Influence of experimental instruments

The monitoring device in our test is an OTDR, type TFP2A. Its spatial resolution is low, about meter level. This is passable to our model tests. However, it is not suitable to be used in field monitoring now. So, the OTDR should be improved. Improving the OTDR will not only enhance the performance of the optical fiber transducer but also make the modeling tests or field monitoring more convenient. Further studies are needed to verify this correlation.

On the other hand, according to the experimental results of the third-generation and fourth-generation transducers, the loss data of optical fiber are too discrete and are extremely inconsistent with the displacement variations because fiber #4 is located at the end of the entire sensing line and far from the OTDR. Thus, the number of survey points connected to the OTDR must not exceed three. Further studies on a new OTDR instrument to improve this drawback are urgent.

### 5.4 Influence of test piece preparation

As for the borehole-based slope stability field monitoring technology, the grouting of the transducer was integrated before sliding occurred. However, to guarantee that the shear loading was subjected better to the test piece in our test, we annularly cut a sliding guide plane in the test piece by using the cutting machine. This process follows the method mentioned in the study of Dennis et al. (2006). Nevertheless, the process used in the Dennis et al. (2006) paper is not exactly the same as the reality. However, this sliding guide plane may change some characteristics of the test piece. Therefore, further study on the test piece without a sliding guide plane is necessary.

### 5.5 Comparison with other photoelectric monitoring technologies

As previously mentioned, we compared the features of the fourth-generation transducer with those of the other transducers in terms of initial measurement precision, sliding distance, dynamic range, unit price, and determination of load direction (Table 5).

Table 5 shows that the fourth-generation transducer is the most effective among all transducer versions because this method has a higher initial measurement precision, a larger sliding distance, and good dynamic range. The unit price of the fourth-generation transducer is also very low. Unlike the other listed methods, the fourth-generation transducer can also judge the loading direction, which is a significant progress compared to the other electro-optic monitoring methods.

### 5.6 Further enhancements for the performance of the combined optical fiber transducer

The COFT is to be used in field monitoring, not only for rockslides but also for soil landslides. The practice process is also very inconvenient in its current stage because a free

fiber was needed between every two fibers, which is limited to the spatial resolution of the OTDR as mentioned in Sect. 5.3. Furthermore, as shown in Table 5, the fourth-generation COFT does not have the largest maximum sliding distance and dynamic range. Therefore, the below enhancements are needed to improve the performance of the newly proposed transducer.

First, the cross-section dimension of the transducer could be enlarged. In our previous study, we theoretically proved that the larger the cross-section dimension is, the larger the sliding distance becomes. Further experiments should be made to verify this theory.

Second, could wavelength division multiplexer (WDM) be introduced into the modeling tests and field monitoring? Thus the free fibers need not be set. Then the practice process will be more convenient. Further analyses and experiments should be carried out to verify this suppose.

## 6 Conclusions

Double and single shearing tests were performed in this study, and a new type of combined optical fiber transducer was invented to overcome the drawbacks that occurred when the third-generation transducer underwent double shearing tests. The results of two shearing tests show that the fourth-generation transducer has good initial measurement precision, a certain sliding distance, and good dynamic range, which indicate that this transducer can monitor shearing deformation. The fourth-generation transducer can determine the loading direction and can overcome numerous deficiencies of other existing photoelectric sensing and monitoring technologies, such as single optical fibers, optical grating, and coaxial cables. These findings indicate that the newly proposed fourth-generation transducer can be used for slope stability monitoring.

*Acknowledgements.* Projects 50808187 and 51178488 were supported by National Natural Science Foundation of China. The authors owe their thanks greatly to Jian Zou and Xiaoyu Wang from the Key Laboratory for Optoelectronic Technology & System of Education Ministry of China, Chongqing University.

Edited by: R. Lasaponara
Reviewed by: four anonymous referees

## References

Dennis, N. D., Ooi, C. W., and Wong, V. H.: Estimating movement of shallow slope failures using time domain reflectometry, in: Proc. TDR 2006, Purdue University, West Lafayette, USA, 17–20 September, Paper ID 41, 16 pp., available at: https://engineering.purdue.edu/TDR/Papers (last access: 2 January 2009), 2006.

Ding, Y., Shi, B., Cui, H. L., Suo, W. B., and Liu, J.: A fiber optic sensing net applied in slope monitoring based on Brillouin scattering, Chin. J. Geotech. Eng., 27, 338–342, 2005.

Higuchi, K., Fujisawa, K., Asai, K., Pasuto, A., and Marcato, G.: Application of new landslide monitoring technique using optical fiber sensor at Takisaka Landslide, Japan, in: 1st North American Landslide Conference, 3–10 June 2007, Vail, Colorado, 1074–1083, 2007.

Iten, M. and Puzrin, A. M.: BOTDA road-embedded strain sensing system for landslide boundary localization, Proc. SPIE, 7293, 1–12, 2009.

Jibson, R. W., Harp, E. L., and Michael, J. A.: A method for producing digital probabilistic seismic landslide hazard maps, Eng. Geol., 58, 271–289, 2000.

Matori, A. N., Mokhtar, M. R. M., Cahyono, B. K., bin Wan Yusof, K.: Close-Range Photogrammetric Data for Landslide Monitoring on Slope Area, in: 2012 IEEE Colloquium on Humanities, Science & Engineering Research, Kota Kinabalu, 3–4 December 2012, Sabah, Malaysia, 398–402, 2012.

Sargand, S. M., Sargent, L., and Farrington, S. P.: Inclinometer – Time Domain Reflectometry Comparative Study: Final Report, Ohio Research Institute for Transportation and Environment, Ohio Department of Transportation, Ohio, 1–4, 2004.

Sun, D. F., Li, H., and Lin, P.: Monitoring land use and landscape changes caused migrant resettlement with remote sensing in Region of Three Gorges of Yangtze River, Trans. Chin. Soc. Agr. Eng., 19, 218–224, 2003.

Tang, T. G., Wang, Q. Y., and Liu, H. W.: Experimental research on distributed fiber sensor for sliding damage monitoring, Opt. Laser. Eng., 47, 156–160, 2009.

Wang, B. J., Li, K., Shi, B., and Wei, G. Q.: Test on application of distributed fiber optic sensing technique into soil slope monitoring, Landslides, 6, 61–68, 2009.

Wang, J. Q. and Wang, Z.: Engineering properties of expandable polystyrene and its application, Geotech. Invest. Surv., 4, 9–12, 2002.

Zeni, L.: Optical fiber distributed sensors: a tool for in-situ structural and environmental monitoring, in: IWL 2009, Rainfall Induced Landslides, 8–10 giugno 2009, Napoli, available at: http://www.corista.eu/Docs/opticalfiber.pdf (last access: 11 October 2013), 2009.

Zhu, Z. W., Liu, D. Y., Yuan, Q. Y., and Dong, Q.: Application of electro-optic technology in slope stability monitoring, Piezoelect. Acoustoopt., 31, 112–114, 2009.

Zhu, Z. W., Liu, D. Y., Yuan, Q. Y., Liu, B., and Liu, J. C.: A novel distributed optic fiber transduser for landslides monitoring, Opt. Laser. Eng., 49, 1019–1024, 2011.